Int. J. Electrochem. Sci., 12 **(2017)** 7154 – 7165, doi: 10.20964/2017.08.14

International Journal of
ELECTROCHEMICAL
SCIENCE
www.electrochemsci.org

Nitrogen-doped Graphene Sheets Prepared from Different Graphene-Based Precursors as High Capacity Anode Materials for Lithium-Ion Batteries

Ming-Hua Jiang, Dandan Cai[*], *Ni Tan*

School of Chemistry and Pharmaceutical Sciences, Guangxi Normal University, Key Laboratory for the Chemistry and Molecular Engineering of Medicinal Resources (Ministry of Education), Guilin, 541004, P. R. China.
[*]E-mail: caidandan86@163.com

Received: 1 May 2017 / *Accepted:* 2 June 2017 / *Published:* 12 July 2017

The nitrogen (N) doping in graphene-based materials has been considered as an effective approach to improve the lithium storage performance of lithium-ion batteries. Thus, the studies of the influence of N-doped graphene from different precursors on lithium storage properties are urgently needed. Herein, three different N-doped graphene sheets (N-GT, N-GN, N-RGN) anode materials of LIBs was prepared using the graphite oxides, graphene oxides and reduced graphene oxides as precursors respectively and thermal annealing with melamine. Microstructure tests show the N-RGN possess higher specific surface area (687.7 m^2 g^{-1}), larger interlayer distance and more active sites due to the expanded graphene layers of reduced grapheme oxides than N-GT or N-GN. Electrochemical experiments results show that the order of lithium storage properties is N-RGN > N-GN > N-GT based on specific capacity and cycle performance, which can be explained for specific surface area of material as one of the key structural parameters. Moreover, a high initial reversible capacity of 1250.8 mAh g^{-1} can be achieved for N-RGN at a current density of 100 mA g^{-1}.

Keywords: N-doped graphene; Thermal annealing; Different precursors; Anode materials; Lithium-ion batteries.

1. INTRODUCTION

Lithium-ion batteries (LIBs) have been widely used as the power source for portable electronics due to their high-energy density, good cycle performance and excellent safety. The capacity and cycling stability of LIBs could be improved by seeking the novel high capacity and cycling stable cathode or anode materials [1]. Nowadays, graphite is the most commonly used anode material in

commercial LIBs. However, the theoretical capacity is only 372 mAh g^{-1}, thus severely limiting the further application of LIBs in hybrid electric vehicles and electric vehicles [2].

Graphene, a carbon monolayer packed into a 2D honeycomb lattice, has spurred extensive interest as an anode material for LIBs because of their superior electronic conductivity, low cost, chemical and mechanical stability [3-5]. The capacity of graphene is greatly dependent on its specific surface areas, pore structure, doping and interlayer distance. Following this strategy, various strategies have been developed, such as the design of graphene foam [6], assembly with the assistance of templates [7], the recombination of graphene and carbon nanotube [8] and introduction of heteroatoms into graphene lattice [9]. Among them, nitrogen doping has been an effective way to improve the lithium storage properties of graphene for LIBs [10-15]. As well known, N-doping would further promote the electrochemical performance of graphene electrode, which could be attributed to the more active sites induced by doping, the increased specific surface areas and better electrode/electrolyte wettability [16-19].

To date, N-doped graphene materials can be obtained by various methods including chemical vapor deposition (CVD) [10], hydrothermal [20], plasma treatment [21], arc-discharge approach [22] and thermal treatment with ammonia (NH_3) [11, 16, 17] et al. For example, Reddy et al. first reported the N-doped graphene film prepared by CVD exhibited higher capacity than pristine graphene [10]. Then, Cheng's group synthesized N-doped graphene nanosheets by heat treatment of graphite oxide in an NH_3 atmosphere. The N-doped graphene exhibited high reversible capacity (~1040 mAh g^{-1} at 50 mA g^{-1}) [11]. Cui's group and Sun's group reported that N-graphene sheets were synthesized by a similar heat treatment method. The main difference of the above materials is the using of various graphene-based precursors, and resulting in the different electrochemical performance [16, 17]. Recently, Shen's group reported that N-graphene was assembled by resin-based methodology and exhibited a reversible capacity of 1177 mA h g^{-1} at a current of 50 mA g^{-1} [13]. In addition, N-doped graphene has been prepared by a simple one-step hydrothermal approach using hexamethylenetetramine as single carbon and nitrogen source and showed a reversible capacity of 1420 mAh g^{-1} [20]. Notably, N-doped graphene prepared from different synthetic methods shows diversity in the aspect of the contents of nitrogen and structures, leading to the difference in the lithium storage properties, which renders the principal influence factors are difficult to be determined [23, 24]. Thus, the choice of appropriate methods to control the structure of N-doped graphene is essential. What's more, the thermal annealing method has features of the low cost, easy control, large-scale synthesis and less affected factors [11, 12, 14-18]. Therefore, it is very necessary to study the influence factors of lithium storage properties of N-doped graphene sheets obtained from different precursors by thermal annealing.

Based on the above considerations, different N-doped graphene sheets were synthesized by thermal annealing method using three precursors (graphite oxides, graphene oxides and reduced graphene oxides) and melamine. The microstructure and morphologies were characterized by X-ray diffraction, Brunauer-Emmett-Teller measurements, Raman spectra and scanning electron microscopy. Moreover, the electrochemical performances of N-doped graphene were evaluated as anode material for LIBs.

2. EXPERIMENTS

2.1. Preparation of three different nitrogen-doped graphene sheets

a) Graphite oxide sheets (GTOs) were prepared through the modified Hummer's method [25]. Typically, 1 g of the graphite flakes and 1 g $NaNO_3$ were added into 55 mL of H_2SO_4 with constant stirring at room temperature to form a mixture. The temperature of the mixture was reduced to 0 ^oC, and 6 g $KMnO_4$ was introduced slowly in portions under vigorous stirring for 1 h, and then the reaction temperature was increased to 40 ^oC with stirring for 3 h. The mixture was diluted with 82 mL of ultrapure water and 25 mL of 30% H_2O_2 were added under stirring. The mixture was collected by filtration and washed with 6% H_2SO_4/1% H_2O_2 solution and 5% HCl solution for several times, then subjected to dialysis to completely remove metal ions and acids until the pH was close to neutral. Finally, the GTOs powders were collected by vacuum-drying.

b) Graphene oxide sheets (GNOs) were produced by ultrasonic exfoliation of the received GTOs in deionized water for 2 h and dried in vacuum at 60 ^oC.

c) Reduced graphene oxide sheets (RGOs) were synthesized by thermal reduction of GTOs.

d) Nitrogen-doped graphene sheets were synthesized by a simple thermal annealing approach using the above precursors. First, the GTOs, GNOs or RGOs and melamine were mixed together with a weight ratio of 1:6 by grinding. These mixtures were then calcined at 700 ^oC for 1 h in a tubular muffle furnace under nitrogen gas atmosphere. Finally, the furnace was naturally cooled to room temperature.

In this paper, the above obtained nitrogen-doped graphene sheets was denoted as "N-GT", "N-GN" and "N-RGN", respectively.

2.2. Characterization of materials

The crystal structures of the nitrogen-doped graphene sheets were characterized by X-ray diffraction (XRD) (PHILIPSPW1710) using Cu/K_a radiation and Raman spectra (a Horiba Jobin Yvon LabRam Aramis Raman spectrometer with a laser of 632.8 nm). Elemental analysis was measured with pure oxygen combustion method (vario EL III elementar, Germany). The nitrogen adsorption/desorption isotherms and pore size distribution were measured by using Micromeritics analyzer ASAP 2020 (USA) at liquid nitrogen temperature (77 K). The morphology was characterized by field emission scanning electron microscopy (FE-SEM) (JSM-6330F).

2.3. Electrochemical measurements

The lithium storage properties of the three nitrogen-doped graphene sheets as anode materials were investigated using coin cells (CR2032). The working electrodes were prepared by well dispersed the active materials (N-GT, N-GN and N-RGN), acetylene black, and poly(Vinylidene fluoride) binder (PVDF, Kureha, Japan) in a weight ratio of 75:15:10 in N-methyl-2-pyrrolidone (NMP, Tianjin Kermel Chemical Reagent Co., Ltd., China) to form a slurry. The slurry was pasted on a copper foil

and dried in vacuum oven at 80 ^{o}C for 6 h, followed by pressing. Highly pure lithium foil was used as the counter and reference electrodes. Meanwhile, the celgard 2325 membrane was used as the separator. The electrolyte was $LiPF_6$ (1 mol L^{-1}) dissolved in a mixture of ethylene carbonate (EC) and diethylcarbonate (DEC), with a volume ratio of 1:1. The coin cells were assembled in an argon-filled glove box (Mikrouna, super 1220) in which the content of the oxygen and water both below 1 ppm. The galvanostatic charge/discharge measurements were tested at a current density of 100 mA g-1 using a Battery Testing System (Neware Electronic Co., China) in the voltage range from 0.01 to 3 V vs. Li/Li^{+}.

3. RESULTS AND DISCUSSION

3.1. Microstructural characterization

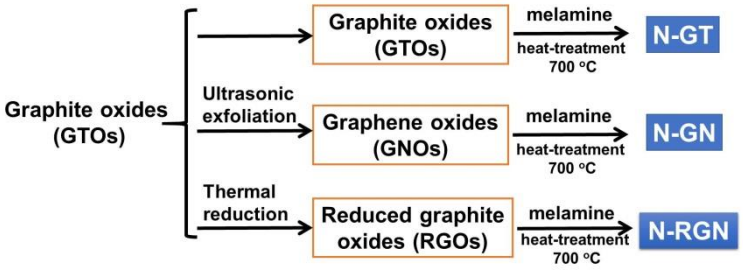

Scheme 1. Synthesis procedures for three kinds of N-doped graphene sheets.

The synthesis procedures of three N-doped graphene sheets are illustrated in Scheme 1. Generally, they involve two steps: (1) preparation and choice of graphene-based precursors (GTOs, GNOs and RGNs) and (2) subsequently heat-treatment of different precursors with melamine to N-doped graphene sheets (N-RT, N-RN and N-RGN, respectively).

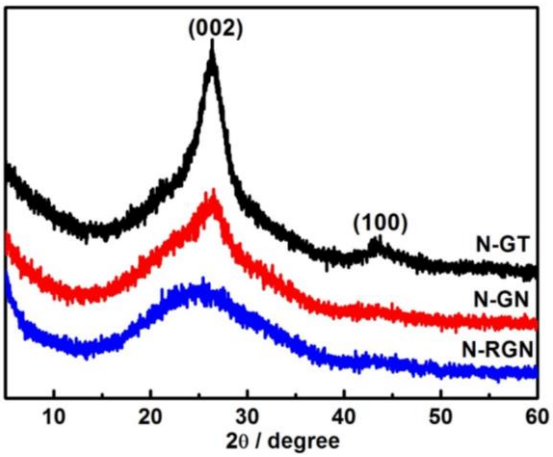

Figure 1. XRD patterns of N-GT, N-GN and N-RGN.

Figure 1 presents the XRD patterns of the three as-fabricated N-doped graphene sheets (N-GT, N-GN and N-RGN). For N-GT, two characteristic peaks were obtained at about $2\theta = 26.2^{o}$ and 43.3^{o} corresponding to the (002) and the (100) plane of graphite, respectively [19, 20]. Meanwhile, the XRD patterns of N-GN and N-RGN exhibit similar diffraction features with one broader (002) peak may be due to the more corrugation and defects structure of the N-doped graphene sheets. These signal peaks indicate that interlayer spacing of the N-GT, N-GN and N-RGN is larger than that of graphite. The interlayer spacing (d_{002}) was calculated from Braggs' law ($d = n\lambda/2\sin\theta$) [26, 27]. The d_{002} spacing of the N-RGN are about 0.358 nm, which is larger than the spacing of N-GN (d_{002} = 0.342 nm) and N-GT (d_{002} = 0.339 nm). The enlarged d_{002} spacing is beneficial to the reversible lithium ions insertion/extraction owing to the lower energy barrier, which is consistent with the previous reports in the literature [19, 20, 24, 26].

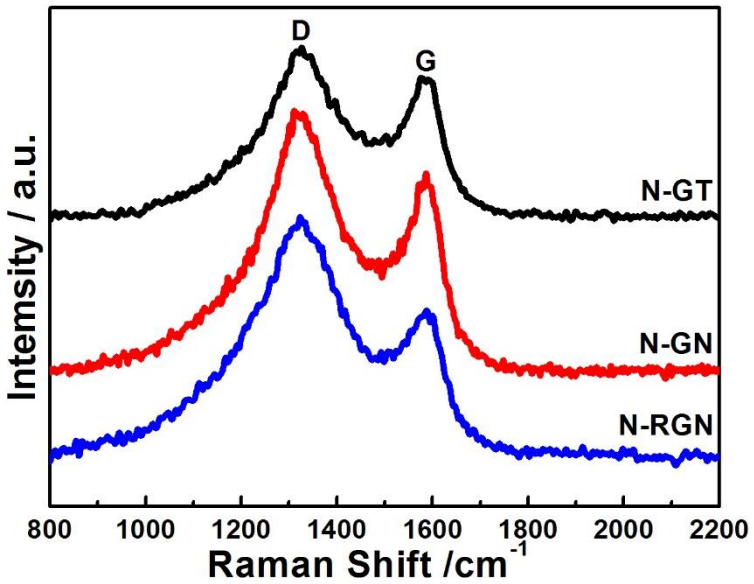

Figure 2. Raman spectra of N-GT, N-GN and N-RGN.

Raman spectra are considered as an effective tool to detect the microstructure of the N-doped graphene-based materials [11, 12, 14]. The Raman spectra of the N-GT, N-GN and N-RGN are displayed in Figure 2. For all three N-doped graphene sheets, D band (1326.2 cm^{-1}) and G band (1586.9 cm^{-1}) can be observed, which were obvious peaks of graphene-based materials [16-20]. It is well known that the G band with E_{2g} symmetry is related to the ordered sp^2 carbon materials and the D band with A_{1g} symmetry is ascribed to disordered carbon, edge defects, sp^3 bonded carbon, dangling bonds, vacancies, and topological defects [18-20]. Thus, the intensity ratio of D band to G band (I_D/I_G) indicates the presence of structural defects in the N-doped graphene sheets layers. As shown in Figure 2, the N-RGN shows apparently higher I_D/I_G (1.70) than the N-GT (1.09) and N-GN (1.25), suggesting that the as-obtained N-doped graphene using reduced graphene oxides as precursors could significantly generate more extrinsic defects.

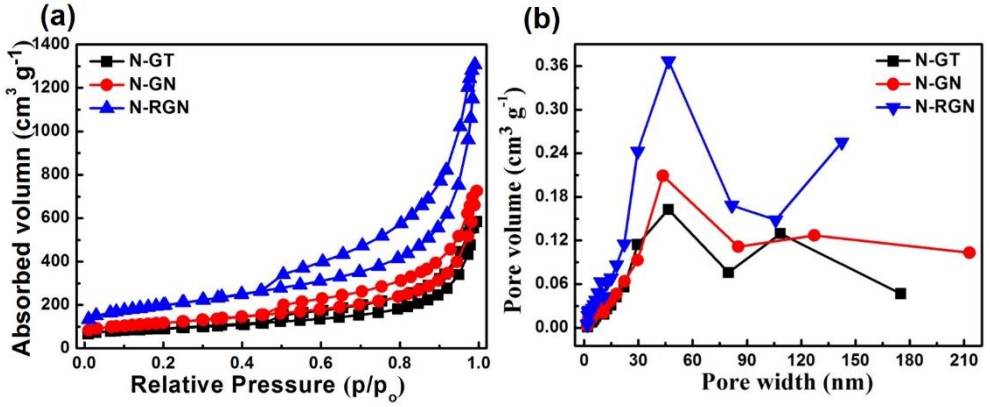

Figure 3. (a) N_2 adsorption/desorption isotherm and (b) the pore size distribution of the N-GT, N-GN and N-RGN.

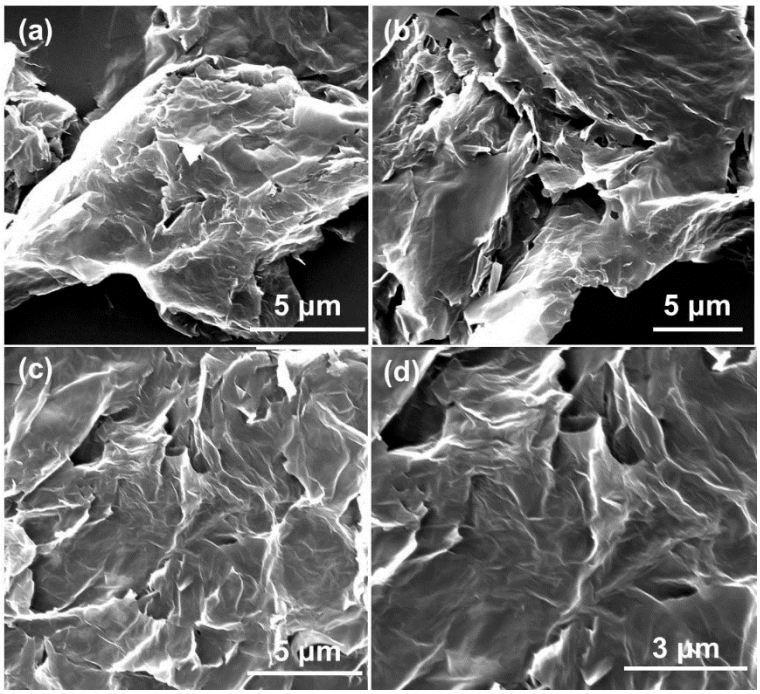

Figure 4. SEM images of (a) N-GT, (b) N-GN and (c, d) N-RGN

Figure 3 shows N_2 adsorption/desorption isotherms and the pore characteristics of the N-GT, N-GN and N-RGN. For the three N-doped graphene, the isotherms all shows type IV adsorption/desorption behavior with an H_4 hysteresis loop, implying the existence of micropores and mesopores [18, 26]. The specific surface area of N-doped graphene is calculated by the multi-point BET method. For N-RGN, the BET surface area is up to 687.7 m^2 g^{-1}, which is much large than those of N-GT (311.9 m^2 g^{-1}) and N-GN (405.5 m^2 g^{-1}). The higher specific surface area is attributed to the leaving of oxygen atom by heat treatment and defects induced by N-doping. The larger specific surface area might be one of the reasons for the higher irreversible capacity. The Barrett-Joyner-Halenda (BJH) pore size distribution (Figure 3b) reveals that the three N-doped graphene possess mesopores with a size distribution at about 46 nm. These pores might be formed by the random stacking of the N-

doped graphene sheets and the thermal reducing during the process of N introducing into graphene lattice [11, 12, 14, 15].

The morphologies of N-GT, N-GN and N-RGN are shown in Figure 4. The SEM images show that N-GT and N-GN have a thick and overlapped sheet structure. The N-RGN still maintains the typically wrinkled morphology of graphene sheets and has more corrugations and scrolling than N-GT and N-GN. Moreover, N-RGN sheets are randomly distributed and overlapped to form a flexible interconnected conducting network. The N-GT and N-GN tend to aggregate presumably due to the formation of hydrogen bonds between the pyrrole -NH and hydroxyl –OH groups of graphene edge [11, 16, 17, 28, 29]. The nitrogen relative contents of the three N-doped graphene were obtained by quantitative elemental analysis. The results show that the relative elemental percentage of N in the N-RGN is 7.52 %, which is lower than that in N-GT (11.36 %) and N-GN (12.06 %). The higher nitrogen percentage of N-GT and N-GN could be attributed to the more oxygenous groups linked to graphene nanosheets in the GTOs and GNOs. During the possible N doping process, oxygen groups linked to graphene nanosheets in graphene-based precursors were removed at high temperature, then the removal process of oxygen species provides active sites for nitrogen doping into graphene frameworks [12, 30-32].

3.2. lithium storage properties of the three nitrogen-doped graphene sheets

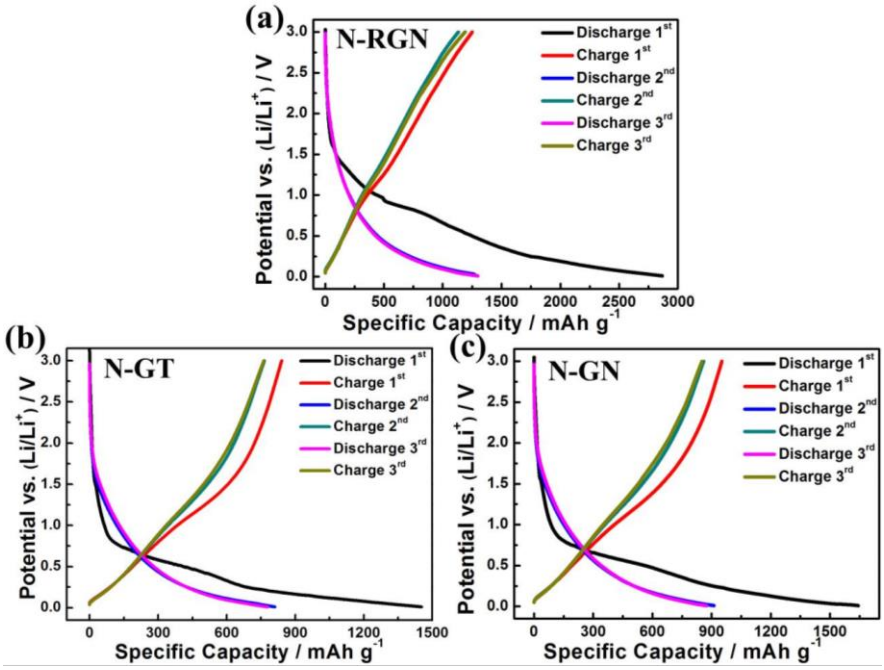

Figure 5. Galvanostatic discharge/charge profiles of the three N-doped graphene electrode at a current density of 100 mA g^{-1} between 3.0 and 0.01 V versus Li^+/Li.

To evaluate the lithium storage properties of the three N-doped graphene sheets as the anodes for LIBs, their galvanostatic discharge/charge behaviors at a current density of 100 mA g^{-1} were measured in a coin-type cell. The first three discharge/charge profiles of the N-RGN, N-GT and N-GN

at a current density of 100 mA g^{-1} between 3.0 and 0.01 V versus Li^+/Li are shown in Figure 5a, b and c, respectively. For the three N-doped graphene sheets, the intercalation of lithium ions of the first cycle begins at around 2.0 V versus Li^+/Li. Additionally, the curve exhibits a slope plateau at 0.7 V which is attributed to the combination of lithium ions adsorption on the structural defects of the N-doped graphene layers and the formation of solid electrolyte interphase (SEI) film on the surface of the N-doped graphene electrodes [11-13, 33]. As we can see from the discharge/charge curves of the three N-doped graphene, there is no distinct plateau below 0.3 V, due to the presence of a large amount of disordered carbon atoms [2, 5, 25, 29]. The results suggest that the more disordered carbon structure of N-GRN was observed, which is consistent with the result of Raman spectra.

The N-RGN exhibit a reversible capacity of 1250.8 mAh g^{-1} in the first cycle which are significantly higher than those of the N-GN (951.6 mAh g^{-1} in the first cycle) and N-GT (840.4 mAh g^{-1} in the first cycle) electrodes. Moreover, compared to the theoretical discharge capacity (372.0 mAh g^{-1}) of graphite, the three N-doped graphene sheets show a remarkable promotion of the capacity, indicating the different lithium storage mechanism for graphene and graphite as the anode materials for LIBs [2, 28]. Notably, the Coulombic efficiency (43.62 %) of the N-RGN are lower in comparison with N-GT (57.88 %) and N-GN (57.86 %). The irreversible capacity loss could originate from the electrolyte decomposition, the formation of SEI layer at the electrode surface or the strong lithium ions adsorption on the special positions like vicinity or vacancies of oxygen and nitrogen groups [11-13]. The N-RGN with more disorder degree tend to result in the electrolyte decomposition and surface side reactions of N-doped graphene electrodes with the electrolyte. The Coulombic efficiency of the second discharge/charge cycle is 94.1 %, which is further increased to 97.3 % in the third discharge/charge cycle, indicating an improved reversibility of the lithium-ions intercalation/detercalation stability.

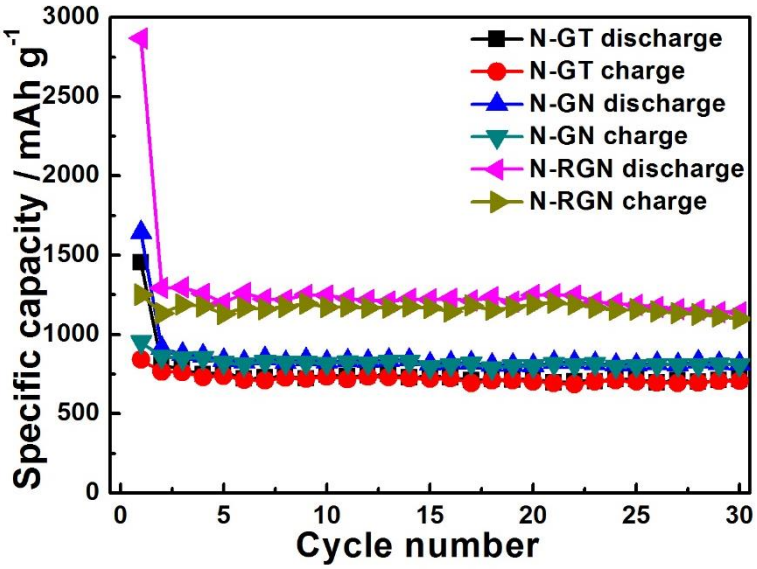

Figure 6. Cycling performances of N-GT, N-GN and N-RGN at a current density of 100 mA g^{-1}.

Figure 6 presents the comparative cycling performances of N-GT, N-GN and N-RGN at the current density of 100 mA g^{-1} between 0.01 and 3.0 V versus Li^+/Li for 30 cycles. The N-doped

graphene sheets derived from RGOs have improved reversible specific capacity of 1095.2 mAh g^{-1} over 30 cycles, still much higher than that of N-GT (808.9 mAh g^{-1}), N-GN (707.1 mAh g^{-1}) and the theoretical capacity of graphite. Consequently, the reversible specific capacity retention is increased from 84.1% for the N-GT to 85.0 % for the N-GN and to 87.9 % for the N-RGN after 30 cycles. The high and stable capacities indicate high capacity retention of the three N-doped graphene sheets electrode. Moreover, the N-RGN sheets exhibit better cycling stability and higher specific capacities than the N-GT and N-GN.

The comparison of the synthesis, microstructure and lithium-ion storage properties of N-doped graphene in the previous literatures is shown in Table 1. It is found that N-doped graphene synthesized by different methods presented the different lithium storage properties. The distinction of lithium storage perforamce could be attributed to the special microstructure and chemical composition, such as spefic surface area, interlayer spacing, disorder degree and nitrogen content et al. For example, the incorporation of template method and heat treatment method could create more micropores and mesopores [15, 24], which shorten the transfer distance of lithium ions and increase the permeability of the electrolyte, improving the electrochemical performance of LIBs. According to the above results, the influence of the microstructure and nitrogen content on the lithium storage properties of the N-doped graphene materials could be summarized as follows. 1) N_2 adsorption/desorption measurement shows the specific surface area of N-RGN is much larger than that of N-GT or N-GN. What's more, the electrochemical results show that N-RGN exhibits the highest specific capacity among the three N-doped graphene sheets. The results suggest that the specific capacity of LIBs could be improved by increasing the specific surface area of materials, which is consistent with the previous reports [14, 15, 18-20]. It has also been demonstrated that the existence of micropores could also contribute to the improved discharge capacity of the N-doped graphene sheets [18]. In addition, the Nitrogen-doped holey graphene hollow microspheres with highest specific surface area (948 m^2 g^{-1}) could exhibit the highest specific capacity of 1923 mAh g^{-1} among the previous reported N-doepd graphene anode materials [24]. 2) There should be little difference among the interlayer spacing of N-RGN, N-GN and N-GT, so the slight influence of the interlayer spacing on lithium storage properties for the N-doped graphene. 3) Although the nitrogen content of N-RGN is lower than that of N-GN or GT, the N-RGN exhibits higher reversible capacity. It has been reported that the nitrogen doping level can increase the lithium storage performance of N-doped graphene in the similar conditions [11, 12, 32]. However, it could be found that the specific capacity (539 mAh g^{-1} at 50 mA g^{-1}) of N-doped graphene with 3.15 % nitrogen content is obvious lower than that of N-doped graphene with 1.68 % nitrogen content (950 mAh g^{-1} at 100 mA g^{-1}) [19, 20]. The higher capacity could be explained by N-doped graphene with low N content possessing higher specific surface area (466 m^2 g^{-1}) [19, 20]. Therefore, the results suggest that the specific surface area might be one of the key structural parameters for the lithium storage capacity of N-doped graphene sheets.

Table 1. Comparison of synthesis, microstructure and lithium-ion storage properties of N-doped graphene in the previous literatures

Materials	Synthesis method	The content of nitrogen (at%)	Spscific surface area (m^2 g^{-1})	*d* spacing (nm)	Initial capacity (mAh g^{-1})/Current density (mA g^{-1})	Capacity retention (mAh g^{-1})/ cycles (numbers)	Ref.
N-doped graphene	Heat treatment	3.06	290	-	1040/50	872/30	[11]
N-doped graphene	Heat treatment	7.04	-	-	1123/50	1136/50	[12]
N-self-doped graphene	Resin-based methodology	2.1	-	0.342	1177/50	682/95	[13]
N-3D GFs [a]	Sacrificial template and heat treatment	2.02	281.42	-	974/200	1094/100	[15]
NGS [b]	Heat treatment	2	-	-	900/42	-	[16]
N-GNS [c]	Heat treatment	2.8	599	-	-	684/501	[17]
NGHSs [d]	Heat treatment	9.37	574	-	1722.6/100	1370.2/50	[18]
N-doped graphene	Ball-milling	3.15	127.1	0.35	539/50	550/100	[19]
N-doped graphene	Hydrothermal approach	1.68	466	0.34	950/100	600/50	[20]
NHGHSs [e]	Template sacrificing method	9.63	948	0.41	1923/100	1636/50	[24]
N-GT	Heat treatment	12.36	311.9	0.339	840.4/100	707.1/30	this work
N-GN		13.86	405.5	0.342	951.6/100	808.9/30	
N-RGN		8.52	687.7	0.352	1250.8/100	1095.2/30	

[a] N-3D GFs = N-doped 3D graphene frameworks

[b] NGS = N-doped graphene nanosheets

[c] N-GNS = N-doped graphene nanosheets

[d] NHGHSs = N-doped holey graphene hollow microspheres

[e] NGHSs = N-doped graphene hollow microspheres

4. CONCLUSIONS

In summary, GTOs, GNOs and RGOs were chosen as graphene-based precursors with melamine by thermal annealing to synthesize three kinds of N-doped graphene sheets (N-GT, N-GN and N-RGN). The microstructural characterization show that the N-RGN possess highest specific surface area, largest interlayer distance and most active sites among the three N-doped graphene. Moreover, the order of lithium storage properties is N-RGN > N-GN > N-GT. The N-RGN exhibits a high initial reversible capacity of 1250.8 mAh g^{-1} and maintains in the capacity of 1095.2 mAh g^{-1} after 30 cycles at a current density of 100 mA g^{-1}. According to the comparison of microstructure and electrochemical properties, the specific surface area could be a crucial influence factor for the lithium storage capacity of N-doped graphene sheets. The experiments and results could be helpful for studying the lithium storage mechanism and developing the high-performance N-doped graphene electrode materials for LIBs.

ACKNOWLEDGEMENTS
This work was financially supported by the National Natural Science Foundation of China (No. 21661008), Guangxi Natural Science Foundation (No. 2015GXNSFBA139025), the Science and Technology Research Project of Guangxi Universities (No. KY2015YB035) and the Program for Key Scientific Research of Guangxi Normal University (2014ZD006).

References

1. N.S. Choi, Z. Chen, S.A. Freunberger, X. Ji, Y.K. Sun, K. Amine, G. Yushin, L.F. Nazar, J. Cho and P.G. Bruce, *Angew. Chem. Int. Ed.*, 51 (2012) 9994.
2. N.A. Kaskhedikar and J. Maier, *Adv. Mater.*, 21 (2009) 2664.
3. E.G. Leggesse, C.-L. Chen and J.-C. Jiang, *Carbon*, 103 (2016) 209.
4. R. Raccichini, A. Varzi, S. Passerini and B. Scrosati, *Nat. Mater.*, 14 (2015) 271.
5. S. Wu, R. Xu, M. Lu, R. Ge, J. Iocozzia, C. Han, B. Jiang and Z. Lin, *Adv. Energy Mater.*, 5 (2015) 1500400.
6. T.M. Paronyan, A.K. Thapa, A. Sherehiy, J.B. Jasinski and J.S. Jangam, *Sci. Rep.*, 7 (2017) 39944.
7. D. Cai, L. Ding, S. Wang, Z. Li, M. Zhu and H. Wang, *Electrochim. Acta*, 139 (2014) 96.
8. E. Yoo, J. Kim, E. Hosono, H.-s. Zhou, T. Kudo and I. Honma, *Nano Lett.*, 8 (2008) 2277.
9. X. Wang, G. Sun, P. Routh, D.H. Kim, W. Huang and P. Chen, *Chem. Soc. Rev.*, 43 (2014) 7067.
10. A.L.M. Reddy, A. Srivastava, S.R. Gowda, H. Gullapalli, M. Dubey and P.M. Ajayan, *ACS nano*, 4 (2010) 6337.
11. Z.-S. Wu, W. Ren, L. Xu, F. Li and H.-M. Cheng, *ACS nano*, 5 (2011) 5463.
12. D. Cai, S. Wang, P. Lian, X. Zhu, D. Li, W. Yang and H. Wang, *Electrochim. Acta*, 90 (2013) 492.
13. C. He, R. Wang, H. Fu and P.K. Shen, *J. Mater. Chem. A*, 1 (2013) 14586.
14. X. Wang, L. Lv, Z. Cheng, J. Gao, L. Dong, C. Hu and L. Qu, *Adv. Energy Mater.*, 6 (2016) 1502100.
15. X. Liu, Y. Wu, Z. Yang, F. Pan, X. Zhong, J. Wang, L. Gu, and Y. Yu, *J. Power Sources*, 293 (2015) 799.
16. H. Wang, C. Zhang, Z. Liu, L. Wang, P. Han, H. Xu, K. Zhang, S. Dong, J. Yao and G. Cui, *J. Mater. Chem.*, 21 (2011) 5430.
17. X. Li, D. Geng, Y. Zhang, X. Meng, R. Li and X. Sun, *Electrochem. Commun.*, 13 (2011) 822.
18. Z. Jiang, Z.-J. Jiang, X. Tian and L. Luo, *Electrochim. Acta*, 146 (2014) 455.

19. C. Liu, X. Liu, J. Tan, Q. Wang, H. Wen and C. Zhang, *J. Power Sources*, 342 (2017) 157.
20. Z. Xing, Z. Ju, Y. Zhao, J. Wan, Y. Zhu, Y. Qiang and Y. Qian,*Sci. Rep.*, 6 (2016) 26146.
21. H.M. Jeong, J.W. Lee, W.H. Shin, Y.J. Choi, H.J. Shin, J.K. Kang and J.W. Choi, *Nano Lett.*, 11 (2011) 2472.
22. L.S. Panchakarla, K.S. Subrahmanyam, S.K. Saha, A. Govindaraj, H.R. Krishnamurthy, U.V. Waghmare and C.N.R. Rao, *Adv. Mater.*, 21 (2009) 4726.
23. Y. Liu, X. Wang, Y. Dong, Z. Wang, Z. Zhao and J. Qiu, *J. Mater. Chem. A*, 2 (2014) 16832.
24. Z.J. Jiang and Z. Jiang, *ACS Appl.Mater.Interfaces*, 6 (2014) 19082.
25. P. Lian, X. Zhu, S. Liang, Z. Li, W. Yang and H. Wang, Electrochim. Acta, 55 (2010) 3909.
26. D. Cai, S. Wang, L. Ding, P. Lian, S. Zhang, F. Peng and H. Wang, *J. Power Sources*, 254 (2014) 198.
27. W. Ahn, H.S. Song, S.-H. Park, K.-B. Kim, K.-H. Shin, S.N. Lim and S.-H. Yeon, *Electrochim. Acta*, 132 (2014) 172.
28. H.F. Xiang, Z.D. Li, K. Xie, J.Z. Jiang, J.J. Chen, P.C. Lian, J.S. Wu, Y. Yu and H.H. Wang, RSC Adv., 2 (2012) 6792.
29. S.-L. Kuo, W.-R. Liu, C.-P. Kuo, N.-L. Wu and H.-C. Wu, *J. Power Sources*, 244 (2013) 552.
30. S.-Y. Yang, K.-H. Chang, Y.-L. Huang, Y.-F. Lee, H.-W. Tien, S.-M. Li, Y.-H. Lee, C.-H. Liu, C.-C.M. Ma and C.-C. Hu, *Electrochem. commun.*, 14 (2012) 39.
31. Z.-H. Sheng, L. Shao, J.-J. Chen, W.-J. Bao, F.-B. Wang and X.-H. Xia, *ACS nano*, 5 (2011) 4350.
32. W. Ren, D. Li, H. Liu, R. Mi, Y. Zhang, L. Dong and L. Dong, *Electrochim. Acta*, 105 (2013) 75.
33. F. Liu, S. Song, D. Xue and H. Zhang, *Adv. Mater.*, 24 (2012) 1089.